A TRIDENT SCHOLAR PROJECT REPORT

NO. 522

A Novel Approach to Thermoelectric Material Fabrication Using Additive Manufacturing

by

Midshipman 1/C James J. Potticary, USN

UNITED STATES NAVAL ACADEMY
ANNAPOLIS, MARYLAND

USNA-1531-2

REPORT DOCUMENTATION PAGE

Form Approved
OMB No. 0704-0188

1. REPORT DATE *(DD-MM-YYYY)*	**2. REPORT TYPE**	**3. DATES COVERED** *(From - To)*
5-16-22		

4. TITLE AND SUBTITLE
A Novel Approach to Thermoelectric Material Fabrication Using Additive Manufacturing

5a. CONTRACT NUMBER

5b. GRANT NUMBER

5c. PROGRAM ELEMENT NUMBER

6. AUTHOR(S)
James J. Potticary

5d. PROJECT NUMBER

5e. TASK NUMBER

5f. WORK UNIT NUMBER

7. PERFORMING ORGANIZATION NAME(S) AND ADDRESS(ES)

8. PERFORMING ORGANIZATION REPORT NUMBER

9. SPONSORING / MONITORING AGENCY NAME(S) AND ADDRESS(ES)
U.S. Naval Academy
Annapolis, MD 21402

10. SPONSOR/MONITOR'S ACRONYM(S)

11. SPONSOR/MONITOR'S REPORT NUMBER(S)
Trident Scholar Report no. 522 (2022)

12. DISTRIBUTION / AVAILABILITY STATEMENT

This document has been approved for public release; its distribution is UNLIMITED.

13. SUPPLEMENTARY NOTES

14. ABSTRACT

Recently there has been increased interest in developing thermoelectric materials with additive manufacturing (AM) techniques. Thermoelectric materials can capture waste heat and generate electricity. These materials have not seen widespread application for several reasons including: inefficient material properties, and fabrication difficulties. AM thermoelectric materials have demonstrated lower thermal conductivities, which can be a hallmark of a more efficient thermoelectric device. AM can also be used to create difficult geometries—geometries unobtainable with standard fabrication techniques. The goal of this work was to develop and characterize an AM fabrication method capable of creating dimensionally accurate thermoelectric materials.
N-type bismuth telluride (BiTe) was chosen as the base material due to availability and effectiveness as a room temperature thermoelectric. Initial methods of fabrication used a Formlabs Form2 Printer and a doped resin. Image analysis was done to verify the doping percentage. However, thermoelectric characterization showed that these samples did not exhibit a Seebeck effect and were therefore not functional thermoelectric materials.
Due to the printer's limitations with doped resin, a method labeled bulk curing in plastic AM molds was devised. The maximum concentration achieved was 80wt% BiTeSe. Once sintered, the samples exhibited a measurable thermoelectric effect. Mechanically the materials demonstrated non-homogeneous hardness characteristics.

15. SUBJECT TERMS
Additive Manufacturing, Thermoelectric Material, Bismuth Telluride

16. SECURITY CLASSIFICATION OF:			**17. LIMITATION OF ABSTRACT**	**18. NUMBER OF PAGES**	**19a. NAME OF RESPONSIBLE PERSON**
a. REPORT	**b. ABSTRACT**	**c. THIS PAGE**		26	**19b. TELEPHONE NUMBER** *(include area code)*

U.S.N.A. --- Trident Scholar project report; no. 522 (2022)

A NOVEL APPROACH TO THERMOELECTRIC MATERIAL FABRICATION USING ADDITIVE MANUFACTURING

by

Midshipman 1/C James J. Potticary
United States Naval Academy
Annapolis, Maryland

_____
(signature)

Certification of Adviser(s) Approval

CAPT Brad Baker, USN
Mechanical Engineering Department

_____
(signature)

_____
(date)

Professor Peter Joyce Mechanical Engineering Department	Assoc. Professor Emily Retzlaff Mechanical Engineering Department	Assoc. Professor Hatem ElBidweihy Electrical and Computer Engineering Department
_____ (signature)	_____ (signature)	_____ (signature)
_____ (date)	_____ (date)	_____ (date)

Acceptance for the Trident Scholar Committee

Professor Maria J. Schroeder
Associate Director of Midshipman Research

_____
(signature)

_____
(date)

USNA-1531-2

ABSTRACT

Recently there has been increased interest in developing thermoelectric materials with additive manufacturing (AM) techniques. Thermoelectric materials can capture waste heat and generate electricity. These materials have not seen widespread application for several reasons including: inefficient material properties, and fabrication difficulties. AM thermoelectric materials have demonstrated lower thermal conductivities, which can be a hallmark of a more efficient thermoelectric device. AM can also be used to create difficult geometries—geometries unobtainable with standard fabrication techniques. The goal of this work was to develop and characterize an AM fabrication method capable of creating dimensionally accurate, uniform, thermoelectric materials.

N-type bismuth telluride (BiTe) was chosen as the base material due to availability and effectiveness as a room temperature thermoelectric. Initial methods of fabrication used a Formlabs Form2 Printer and a doped resin. After significant manipulation of printer parameters, a maximum concentration of 15wt% BiTe was successfully printed. Image analysis was done to verify the doping percentage. However, thermoelectric characterization showed that these samples did not exhibit a Seebeck effect and were therefore not functional thermoelectric materials.

Due to the printers limitations with doped resins, two alternative methods were attempted: powder sintering in ceramic molds, and a method labeled bulk curing in plastic AM molds. In the first alternative, ceramic molds were 3D printed and thermoelectric material was sintered within the mold. Ultimately, these samples were too fragile to undergo characterization.

In the bulk curing method, BiTe doped resin was cured without the use of a printer. Instead, samples were cured in AM molds using both time and UV activated, doped resins. After the resin was cured it was burned off and the samples were sintered. The maximum concentration achieved was 80wt% BiTeSe. Once sintered, the samples exhibited a measurable thermoelectric effect. Mechanically the materials demonstrated non-homogeneous hardness characteristics due to porosity.

Key words: *Additive Manufacturing, Thermoelectric Material, Bismuth Telluride*

ACKNOWLEDGEMENTS

MIDN Potticary would like to thank Northrup Grumman for funding this research. Associate Professor Brian Donovan for his assistance in characterizing the thermoelectric material. CDR David Durkin for training and technical advice. Dr. Brandon Wilfong, Marc Bergeron, Machinist Mate First Class Michael Landry, and Formlabs for their technical advice. He is also grateful for the support of the Trident committee throughout the entire project.

CONTENTS

I. Background

A. Thermoelectric Generators

A thermoelectric generator (TEG) is a device that uses a temperature gradient to create electricity. This technology was first theorized in 1826 by Dr. T.J. Seebeck [1]. The theory would be built upon in 1834 by Jean-Charles-Athanase Peltier. By 1912 the first thermoelectric prototype had been created by Edmund Altenkirch [2]. TEGs offer a unique collection of benefits. They have no moving parts, have a small profile, and do not require any outside resources like fossil fuels to power them. TEGs offer a clean method to generate electricity with something that humans have in abundance: waste heat. To capture even a small amount for productive purposes would be monumental.

Unfortunately, TEGs were, and still are, inefficient and difficult to manufacture. Despite this, TEGs have found homes in some consumer, and military applications. Examples of this technology are already on the market. For example, the camp stove in Figure 1a uses sticks and a thermoelectric to create 3 watts of power [3]. Other people have attempted to make watches, or other wearable devices such as the bracelet shown in Fig. 1b, leveraging a temperature gradient from the human body [4]. TEGs even power satellites in space, and weather stations in the Arctic [5]. There are many potential applications for this technology as well. A TEG could be mounted to the exhaust of any internal combustion engine or on a spent nuclear fuel receptacle. Achieving this potential relies on finding simpler manufacturing methods and increasing their efficiency.

(a) Camp stove with a TEG that charges a phone [3] (b) Bracelet that uses a TEG to charge a phone [4]

Figure 1: Applications of TEGs

B. Characterization

1) Thermoelectric Properties: The thermoelectric figure of merit (ZT) is a dimensionless value given to a material that describes the thermoelectric materials (TMats) performance as a generator. Room temperature bulk materials manufactured with conventional methods are typically in the 1-2 range [6]–[8]. Compared to other methods of power generation this low ZT is equivalent to a very inefficient generator. The magnitude of ZT can be calculated using thermal and electrical material properties. ZT is calculated using equation 1, where ρ is the electrical resistivity of a material in $Ohm-meter$, S is the Seebeck Coefficient in $\frac{Volts}{Kelvin}$, κ is the thermal conductivity in $\frac{Watts}{meterKelvin}$, and T is the absolute temperature in Kelvin. It is evident that low values of thermal conductivity and resistivity yield a large ZT.

$$ZT = \frac{S^2 T}{\kappa \rho} \tag{1}$$

The ZT is directly tied to the thermal efficiency (η). Thermal efficiency is a ratio of the work done by system (W_{out}) compared to the heat/work put into it (Q_{in}). This can be seen in equation 2. The typical thermal efficiency of a steam generation power plant might fall in the range of 30-40% and a diesel engine might be 10-15% [9]. Current TEGs, with a ZT of about 1, are in the single digits for thermal efficiency. In order for a TEG to compete with conventional generator, it would need to produce a ZT with a value greater than 3. ZT is tied to the thermal efficiency with the equation given in equation 3 [10]. In equation 3 T_c is the temperature on the cold side, T_h is the temperature on the hot side, and ΔT is the difference between these two. With this equation in mind, it becomes clear that a thermal efficiency is greatest when ZT is largest and when the temperature differential is also large. A ZT of 3 and a ΔT of 227°C gives an efficiency of about 18%.

$$\eta = \frac{W_{out}}{Q_{in}} \tag{2}$$

$$\eta = \frac{\Delta T}{T_h} \frac{\sqrt{1+ZT}-1}{\sqrt{1+ZT}+\frac{T_c}{T_h}} \tag{3}$$

In summary, the best way to optimize efficiency is to optimize ZT . To optimize ZT a small κ and ρ is required (the Seebeck coefficient is related to ρ so it is difficult to increase this value without increasing ρ as well [11]). Therefore, in order to make a practical device, materials need to be obtained and manufactured such that the end product is a thermal insulator and electrical conductor.

2) Mechanical Properties: The thermoelectric characteristics —specifically ZT— of the thermoelectric legs are certainly the most important characteristics. Without these material properties the TEG would be useless. However, the TEG cannot be used if engineers do not understand how the individual components react to mechanical loads. Once values for individual components are known complete TEGs can be modeled using computer software. Strength, hardness and fracture toughness are common metrics for measuring a material's reaction to applied forces. One cannot assume that the properties are consistent across all materials and production methods. As is true with the thermoelectric properties, bulk values are typically altered by the processing techniques used. This is because many processing techniques alter the microstructure of the material. This means that each new method of manufacturing must be characterized.

A characteristic that is used to classify a material is hardness. Hardness is the resistance to localized plastic deformation and is measured by resistance to indentation. It is very helpful in determining how a material will wear over time. Hardness is related to, but independent of, to the strength of the material. Hard materials are typically strong, and vice versa. The Vickers hardness of a typical TMat is about 102 HV [12]. A piece of 1020 steel has a Vickers hardness nearly double that of the thermoelectric at 183.5 HV [13]. Hardness is measured by measuring the size of a standard indent made from an applied load, after the load is removed.

The range of properties mentioned so far are all very helpful to know. However, it is even more helpful to know what drives these properties. The microstructure of a material plays a large role in many of these properties. In ceramics, like those that compose TMats, flaws are the feature that have the greatest effect on the material properties. These ‘flaws’ occur during phase transformation. Both electrical and mechanical properties can be tied back to the microstructure of a material.

These materials are crystalline and made up of grains defined by their crystallographic orientation. Between the grains voids can form. Voids form or disappear in the process of densification or bloating, respectively. Both describe the density and can generally be called porosity. The densification process is self-explanatory: holes in the material are closed and the material is made denser. Bloating is the reverse: holes are created in the material. This makes the material less dense. Porosity can have a dramatic effect on materials hardness and strength. This observation was assigned an experimental equation [14].

Moreover, electrical and thermal properties are also related to porosity. Generally, the lower the number of pores the lower the resistivity, and the greater the number of pores the lower the thermal conductivity [15], [16]. However, materials with many pores have a low thermal conductivity. TMats that contain pores have a lower thermal conductivity, which can be beneficial for their efficiency.

Therefore, TMats require a material that strikes a balance in porosity. It is ideal to have a material that is a thermal insulator and an electrical conductor. In practice bloating is a bigger threat to the function of TMats. This can be seen in Oztan et al’s. analysis of their sintered parts [17], and He et al’s. similar analysis of their annealed parts [18].

C. Fabrication

TMats need to be specifically engineered in order to achieve peak efficiency. In conventional manufacturing, the TMats are cut into small legs, called thermoelectric legs, and soldered in series to the ceramic backbone (called a substrate).

The original patent to manufacture thermoelectric legs was issued to Westinghouse in 1939. It offered a rudimentary means to create a thermoelectric device. This original method involved cold pressing TMats in a jig [19]. With time new methods were developed. In 1997 Panasonic developed a method that is still in use today by Crystal Ltd, as well as other major thermoelectric firms [20]. This method involves taking a hot-pressed plate of TMat, and this plate is then cut into bars. The bars are then coated in a conductive nickel layer, and then cut into the individual elements [21]. This can be seen in Fig. 2.

While this method is great for creating cubic elements, it does not allow for the creation of alternative geometries. Thimont and Leblanc used computational methods to show that different, more complex macro leg geometries can create elements with a lower thermal conductivity and therefore a larger ZT [22]. Thimont and Leblanc modeled geometries such as tapered triangular elements and they found these to produce more power than the standard cubic options. They were able to model the various geometries using bulk material properties and they found that

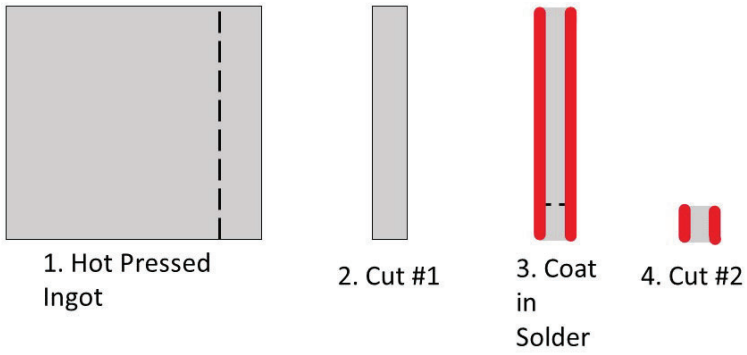

Figure 2: Manufacture Process for Thermoelectric Legs

prism shaped legs exhibited a large electric potential, and were better thermal insulators. In their conclusion they state, “The results presented here point to the strong potential offered by thermoelectric legs with interior voids and hierarchical geometries. However, legs with complex geometries are difficult to achieve with traditional, subtractive manufacturing approaches [22].” They go on to point to AM as a potential solution.

Moreover, the method patented by Panasonic does not easily allow for segmented, or functionally graded legs. A functionally graded leg is a leg designed such that there are different microstructures present throughout the length of the leg. These different microstructures are optimized such that the TEG is more efficient. Shu et al. has experimentally shown a 13.4% increase in power with the use of functionally graded legs [23]. Tian et al. came to a similar conclusion with their functionally graded legs producing up to 72% more power than the non-graded legs [24]. Functionally graded legs can also help TEGs fare better in the face of thermal fatigue. Cramer et al. found that a functionally graded material is more efficient and longer lasting in the face of vigorous thermal cycling [25].

Another disadvantage to the standard cubic leg is that it is a design constraint. A flat leg will not make direct contact with a curved or otherwise difficult geometry, like a pipe. Industrial fabrication methods have not kept up with the technology and simpler methods are needed to make these materials. For this reason, alternative manufacturing methods are under investigation. One such method is additive manufacturing.

Additive manufacturing (AM) offers a solution to the current fabrication problems. It addresses geometry concerns and can be used to create different microstructures throughout a material. AM is defined by the American Society for Testing and Materials (ASTM) as “the process of joining materials to make parts from 3D model data, usually layer upon layer as opposed to subtractive manufacturing and formative manufacturing techniques [26].” Originally conceived and developed for rapid prototyping, creative individuals and organizations have adapted these devices for a multitude of uses. AM has found many practical uses, such as: printing tissue,

medical implants, and custom fit masks for PPE [27], [28]. AM has appeared in many different fields and continues to find new applications. In the field of optics there is Schlichting et al's. creation of tunable lenses [29], and Verploegh et al's. printed wave guides [30]. In the field of material science there has been substantial research in the properties of printed metals. Sridharan et al. used AM to create an $\alpha' + \beta$ phase in a titanium alloy [31], and Carroll et al. have looked at the effect of oxygen presence in the printing process and the effect on the microstructure of metals and their properties [32].

These examples make it clear that AM is not just a novelty. They layout the case for a manufacturing method that is best suited for custom applications, difficult geometries, and parts that are not homogeneously graded. AM has found a niche for custom or unique applications.

The ASTM has defined 7 different types of AM: binder jetting, directed energy deposition, material extrusion, material jetting, powder bed fusion (PBF), sheet lamination, and vat photo polymerization [26]. When the potential to print metals and conventional ceramics began to surface, TMat researchers began to explore adaptations to make AM work for their purpose. The field of TMat research has seen engineers adapt commercial printers to manufacture parts with many of these methods. With most of the focus on powder bed fusion, various thin film methods, fused deposition modeling (FDM- a type of material extrusion), and stereolithography (SLA- a type of vat photo polymerization).

PBF is an AM process that prints using a powder form of the material and a laser (or other energy source like an electron beam). PBF TMat research has shown the capabilities of this technology. Cramer et al. manipulated the grain size of a ZnO thermoelectric to create a more resilient material. They achieved an efficiency of just over 0.6%, this efficiency was sustained even after 20 thermal cycles [25]. El Dosouky et al. were the first to print a non-doped Bismuth Telluride material with a powder bed method. While they did not characterize any of the properties, they demonstrated that it was possible to produce parts using this method [33]. Another study by Thimont et al. has printed Manganese Silicide, and Yan et al. have printed *n* type CoSbTe using a PBF process [34], [35]. Thimont et al. proved that Manganese Silicide could be printed, but did not characterize the thermoelectric properties of the material. The CoSbTe skudderite produced by Yan et al. produced a ZT of 0.56 at 550 °C. Yan et al. did not measure the mechanical properties. Powder bed methods of manufacturing offer serious promise, but most of the work done has simply served as a proof of concept.

Another method commonly used to print TMats is material jetting. Material jetting (MJ) is an AM method that works much like an ink jet printer. It uses a slurry to deposit material on a build plate. Most of the research in this field has been to print thin films on substrates, but some have printed bulk materials as well. Preliminary research has shown that these thin films can be extremely efficient. However, their properties are very difficult to measure and most of the research has been theoretical [36]. Bulk materials have also been processed in this manner. One example is the BiTe thermoelectric generator prototype tested by Madan et al. The maximum ZT obtained was 0.31. The device was not mechanically tested. However, the prototype produced 25 μW with a 20° C temperature differential [37]. Similarly, Su et al. used direct write printing, a type of MJ used to print a bulk thermoelectric device with Bismuth Telluride. It produced a ZT value of 0.11 in the n legs and 0.104 in the p legs. They were also able to model and construct a thermoelectric prototype that wrapped around pipes. However, they did not report the

mechanical properties of their material [38]. Kee et al. created stretchable thermoelectric parts that are also self-healing. Their material had a tensile strength of 3 MPa and produced 2.5 μW of power. Kee et al. proved the practicality of AM organic TMats that could be used in clothing [39].

A third method that is under investigation is the use of material extrusion printers to manufacture TMats. Fused deposition modeling (FDM) is the common method of material extrusion used to manufacture TMats. FDM involves a build plate, an extruder mounted on a gantry, and a filament that is used to create the part. An example of an FDM printer can be seen in Fig. 3. Typically, the build plate moves in the Z direction, and the print head moves in the x-y. Printers also can have two nozzles so that more than one material can be used in a given print. Filaments are typically composed of a thermoplastic base of polylactic Acid (PLA), or acrylonitrile butadiene styrene (ABS). The nozzle is heated to the melting point of the thermoplastic, and filament is fed through it. Some printers even feature a heated build plate to ensure that parts do not detach during the print process. Filaments can be made of almost any material, and these custom filaments have allowed researchers to use FDM to print TMats.

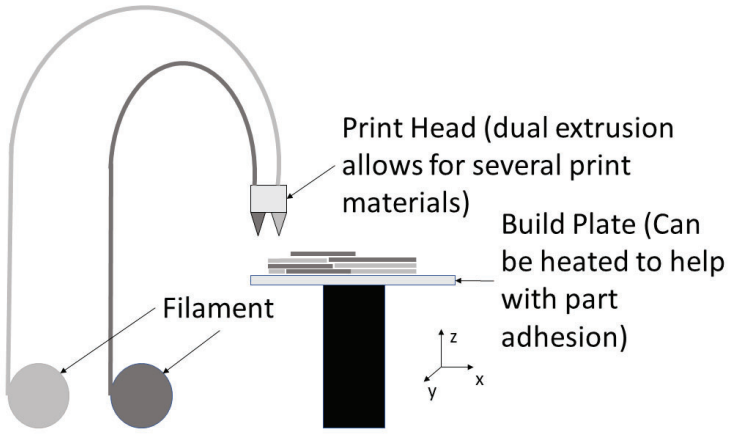

Figure 3: FDM Method of Printing

FDM has been used to print TMats with some success. Oztan et al. printed devices with a ZT value of 0.54. Their filaments were made of ABS and nearly 80wt% Bismuth telluride [17]. Wang et al. used a PLA based bismuth antimony telluride (p type) filament and studied the mechanical and electrical characteristics of the parts. They found that with 81wt% p-type material, they were able to obtain a ZT of 0.011 and a tensile strength of 12 MPa [40]. Finally, Yah Aw et al. studied the mechanical and thermoelectric properties of a ZnO thermoelectric with an CABS base. CABS is a special type of ABS that is electrically conductive. For this reason, they did not post-process their parts which left CABS inside of the material. Because of this, their values for ZT are very low (4.8e-11). However, the systematic manipulation of the print parameters demonstrated that a higher infill yields parts that perform better [41].

Infill is a property that describes the material density below the visible surface. In conventional machining fabrication, the infill is almost always 100% but in AM parts the infill can be

controlled. In the case of a thermoelectric a high infill is good. Even though FDM printers can print 100% infill the layers they create are much thicker than another method known as Stereolithograpy (SLA). The smallest layer thickness of typical FDM printer is 100 microns while SLA printer can print layers that are 25 microns in thickness. Finer layers mean parts with less pores, and fewer pores have been proven to be more ideal for TMats [17], [18], [34], [35], [41]. Moreover, the increased resolution of parts is important if TMats are to be used in engineering applications where dimensional accuracy is important.

The SLA process uses a laser to cure a photoresin layer by layer. This was the first type of 3D printer that was imagined and was patented in 1984 [42]. The process commonly used today is actually the inverse of the original patent, but the idea is still the same. The process can be seen in Fig. 4. A build plate is dipped in a curable resin that is turned from liquid to solid (cured) using a laser. Each time a layer is printed the build plate is moved up slightly, resin is allowed to re-coat the tank, and then the next layer is cured. The tank and resin are enclosed in a UV proof enclosure. This prevents inadvertent curing of the resin. Resin is typically composed of a polymethyl methacrylate (PMMA) base and a photoinitiator.

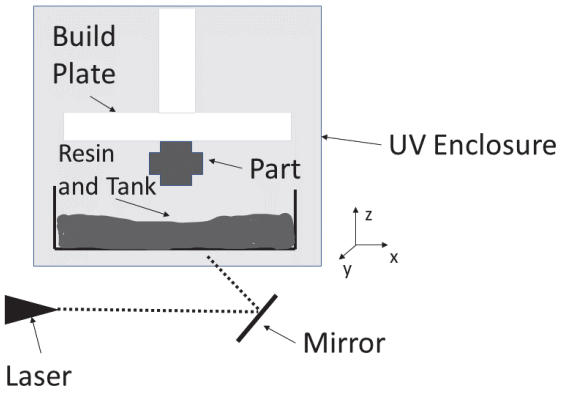

Figure 4: SLA Printer Method

The final step of any SLA process is the post processing. For most conventional applications all that is required is an alcohol wash, but for doped specimens parts need to be sintered and the resin must be burned off. While the polymer resin may provide a lower thermal conductivity, the PMMA base works as an electrical insulator. This is not an ideal characteristic for a thermoelectric. The other purpose of sintering is that the thermoelectric particles are joined closer together. This creates better electrical conductivity and leads to a greater ZT value.

A gauge of success of post processing would be to compare the densities of the final additively manufactured material to hot-pressed versions of the material. Hot-pressed $Bi_{.5}Sb_{1.5}Te_3$ has a reported density of 6.89 g cm^{-3} [8]. Another gauge of success is to analyze the materials molecular and atomic composition of the post-processed material.

When He et al. used their SLA method to create a thermoelectric, they used thermogravimetric analysis to find the ideal temperature to anneal the material, the result was 425°C. When tested on actual printed material, the parts experienced substantial cracking. This led He et al. to anneal their parts at 350°C for varying lengths of time. They found that the parts annealed for 6 hours had the highest density at 2.631 g cm^{-3}. They also found that the grain size dramatically increased with annealing time. Initial grain size was 11 nm and the sample annealed for six hours had a grain size of 67.6 nm [18]. A larger grain, however, is not correlated to enhanced properties. In their analysis of hot pressed materials, Poudel et al. found that the average grain size of their material was 20 nm. This hot pressed material produced a ZT of 1.4. Another example of annealing being used as a post-processing method is seen in the parts created by Su et al. Their direct printed parts underwent an annealing process 6 hours long at 450 °C. The result was a max ZT value of 0.104, and a density of 4.72 g cm^{-3} [38]. The larger density seen in Su et al's study versus that seen in He et al's. research is a product of the different material compositions. The original weight percentage of thermoelectric was 91wt% and 60wt% respectively in these two studies. The removal of plastic clearly has a large impact on the parts density.

Aluminum oxide, silica, silicon nitride and other ceramics have been printed in SLA. Metal powders have also been added to resins and printed with some success. Only one attempt has been found where someone used SLA to print TMat. He et al. printed a TMat using a Formlabs Form1 printer [18]. The TMat manufactured in 2015 produced a ZT of 0.12 and used 60wt% p type Bismuth Telluride. He et al. showed that increasing concentration of Bismuth Telluride increased the ZT.

Substantial research has been done to find what materials are best suited for thermoelectric purposes [43]. Much of that research focuses on adaptations to the *nano* material properties. One material currently being studied is skudderites. Skudderites have cavities in their molecular structure that can hold networks of metal atoms. Metal networks are typically great conductors of electricity. Their high conductivity, and consequently low resistivity, make them good candidates for TMats. Shi et al. has reported ZT values in skudderites as high as 1.7, this is from a κ of 3 W m^{-1} K^{-1}, and a ρ of 2.97e-6 ohm m [44]. Similarly, Kahn et al. achieved a ZT value of 1.6, which was based off a κ of 1.4 W m^{-1} K^{-1}, and a ρ of 8.33 e-6 ohm m [45]. Skudderites are one of many different material structures under investigation, but it is one that has produced some of the highest ZT values. Other material structures include, calthrates, tin and lead chalcogenides, and copper-based materials [46].

The current industry standard for room temperature (200-400 °K) applications is bismuth telluride (Bi_2Te_3) [6]. This material is a binary chalcogenide. Bismuth telluride is made of several layered hexagonal structures with covalent bonds. An example of bismuth telluride is depicted in Fig. 5. In Fig. 5 the hexagonal structure can be seen clearly. *n* doped specimens typically include selenium (Se) and *p* doped variants include antimony (Sb). The nominal compositions of these commercially available materials are $Bi_{.5}Sb_{1.5}Te_3$ for the *p*-type and $Bi_2Te_{2.7}Se_{.3}$ for the *n*-type [6]. For hot pressed ingots a bulk value ZT is typically around 1 [6]. However, manufacturing methods have been shown to alter these values. Poudel et al. found that hot pressed nano crystalline $Bi_{.5}Sb_{1.5}Te_3$ powder produced a peak ZT of 1.4 [8]. Hong et al. manufactured *n*-type bulk materials using a sintering process. They achieved a ZT value of 1.23. The Seebeck coefficient of a typical *n*-type material is -198 μV K^{-1} [7]. Results for these material properties

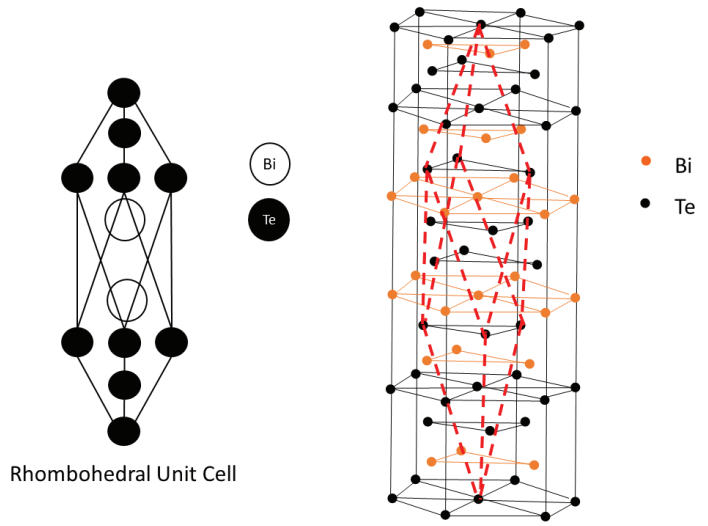

Figure 5: Two visualizations of Bismuth Telluirde Unit Cells- Dashed Lines Highlight Rhombohedral Structure of Unit Cell (Not Drawn to scale)

vary with the manufacturing method of the powder and processing of the powder [47].

The main objective of this study was to develop and evaluate a manufacturing process that allowed for the creation of custom geometries using additive manufacturing. The next objective was to characterize the samples created with this newly developed method.

II. Experimental Methods

Table I details all the fabrication methods and corresponding tests performed. Further detail on each of these processes is detailed in the corresponding section.

Table I: Test Matrix

Fabrication Method	Concentration	Post processing	Tests Performed
SLA Printing	1wt%, 5wt%, 10wt%, 16wt% BiTeSe with Formlabs Clear Resin	IPA Wash and 30 minute UV Cure	PPMS Thermoelectric Characterization, SEM
Free Powder Sintering	100% BiTeSe Powder in an AM mold	None	SEM
Bulk Curing in AM Molds (Light Activated)	60wt% BiTeSe with Formlabs Clear Resin	None	None
Bulk Curing in AM Molds (Time Activated)	80 wt% BiTeSe with West Systems 105 clear epoxy	Sintered at 500 C for 5 hours	Thermoelectric Testing, SEM, Hardness

A. *Fabrication*

1) SLA Printing: Initially parts were printed using a Formlabs Form 2 printer. The Form 2 resin tank was used. This was chosen over the Form 2 Resin Tank LT because Formlabs Ceramic resins are not compatible with the Resin Tank LT. An empty Formlabs Ceramic cartridge was used to make the printer print using the ceramic settings. Ceramic settings differ from other

resins in that the printer incorporates a greater heating temperature and also has an increased wiper frequency.

Two resin formulations were attempted. The first method used vacuum filtration on Formlabs Ceramic resin, in an effort to obtain the resin minus the silica powder.

The second was a composite resin created using Formlabs Clear V4 resin. Clear resin was chosen in favor of a custom recipe due to simplicity. Clear resin also offers the ability to determine if doping occurred. If doping is effective the resin changes color signifying some change. Clear V4 resin was obtained from Formlabs. Parts were laid out and were sent to the printer using Formlabs Cura.

In order for an SLA printer to print Ceramic materials they rely on the dispersion and suspension of ceramic particles in the resin. The suspension of a thermoelectric powder in a resin is difficult due to the density differences that exist between bismuth telluride and PMMA resins. The bismuth telluride is about 7 times (6.89:1) the density of the PMMA which causes it to settle. To combat settling two courses of action were taken: pre-mixing and increased wiper frequency. Pre-mixing involved stirring Formlabs Clear Resin on a hot plate set to 35°C with a stir bar at 300-500 rpm. This resin was then poured into the build tray and spread evenly over the tray. The print was started immediately after mixing in order to prevent settling post-mix. Increased wiper frequency was obtained by using an empty Formlabs Ceramic cartridge. This forced the printer to think that it was printing ceramic materials and therefore increased the frequency of the wiper. Prints were classified as successful if the printer was capable of producing the desired shape without significant operator intervention. The only intervention allowed was the initial start of the print. The highest concentration of powder obtained was 15wt% using this method. Due to the low concentration of TMat in the samples, they were not sintered to remove the plastic binder.

2) Free Powder Sintering: Another fabrication method eliminated the resin altogether. Samples were produced using a purely sintering method. Molds were created using 3d printed ceramics that followed the Formlabs prescribed print and post process procedures for ceramic resin. The thermoelectric powder was then pressed into the molds. The samples were fired at 300 and 500 °C with a 60 °C per hour ramp. The 300 °C samples did not have enough diffusion and lacked structure so the temperature was increased to 500°C. The samples were held at the top of the ramp for one hour. Samples were sintered under a flow of nitrogen gas at atmospheric pressure.

3) Bulk Curing: A final method termed bulk curing was also used. Essentially, AM molds were filled with doped resin and exposed to UV light, or were cured using a West Systems time activated resin. While curing the molds were placed in a vacuum chamber to remove air bubbles introduced during the mixing process. The vacuum needed to be regulated to ensure that the resin did not overflow the molds. Once cured samples were fired in a tube furnace. The furnace was set to increase at 60 °C per hour until the furnace reached 500 °C. Samples were held at 500 °C for 5 hours and then the furnace was allowed to cool down to room temperature. Sintering took place under a nitrogen flow at atmospheric pressure. Samples were doped up to 80wt% using this method.

West Systems 105 Epoxy and 206 Hardener were used for the time cured resins. Thermoelectric materials were obtained from American Elements, in 99.999% purity. They were in a powder

form with a 325 mesh. The Bi_2Te_3 was pre-doped with selenium to obtain N type samples.

B. Microscopy

Samples were imaged using a Tescan Mira3 Scanning Electron Microscope. Samples with lower than 80wt% composition were sputter coated in gold in order to improve conductivity. All samples were viewed under 20kV at a working distance of 15 mm. A backscatter electron detector and energy dispersive X-ray spectroscopy were used to analyze the composition of the samples. Despite the sputter coating, the peaks of bismuth and tellurium are distinct enough from those of gold to allow this method to work. Elements with a high atomic numbers emit backscatter electrons more strongly than light elements. This made the carbon and the bismuth telluride distinguishable. Microscopy and image thresholding were also used to evaluate the effectiveness and reliability of the fabrication processes. 6 representative images were taken of the 5wt% , 15wt%, 80wt% samples. Using ImageJ the images were made binary and an area percentage was calculated to compare to expected values for area percentage.

C. Mechanical Characterization

Hardness values were obtained using the Vickers hardness indenter. The ASTM C1327-15 standard was followed. A Wilson Tukon 1202 was used with a sample polished with 3000 grit sandpaper and dimensions 2x6x12mm (t x w x l). The samples were indented with a 15 second dwell time and 0.5 kgf load. Indents were no closer than two diagonals. This deviation from the standard was made because the porosity of the material was such that there were limited spaces for indents. The 0.5 kgf was used because greater forces created very large indents that were not as easily measured using our system.

D. Thermoelectric Characterization

To measure the thermoelectric figure of merit a sample with nominal dimensions of 2x6x12mm (t x w x l). This sample was then tested using the Physical Property Measurement System and the Thermal Transport Option. A representative sample geometry with leads is shown in Fig. 6. Copper leads were attached with Silver-Filled H20E from Epoxy Technology, Inc. The device measures the thermal conductivity, the resistivity and the Seebeck coefficient over a range of temperatures.

Due to equipment availability, tests were also conducted using a system composed of a laser, a multimeter, and an infrared camera. The custom-built setup provided qualitative data on the existence of a Seebeck effect. A FLIR SC8300HD Camera was positioned above the sample. The sample had two leads connected to it, to measure the voltage. The laser was steered by a total of 5 mirrors, 3 to bring the laser to the correct height, and 2 to move it into location. the laser was also passed through a neutral density filter with an optical density of 0.4. The experimental setup can be seen in Fig. 7. The laser was steered onto its final path using a dichroic mirror. The laser power was incrementally increased until the material underwent a phase change at 2.1 Watts. Temperature gradients and corresponding steady state voltages were collected, and then used to produce loose values for the Seebeck effect. The temperature at the leads was determined

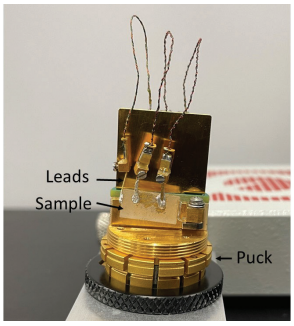

Figure 6: Representative Thermoelectric Sample Attached to PPMS TTO Puck with Leads

using the same pixel location on every sample and then referencing the temperature at that point from the accompanying CSV file. With the two temperatures in hand the difference was found and the steady state voltage reading was divided by the temperature difference. To check the validity of the test method a piece of silica-based ceramic was placed between the leads and was exposed to the laser. There was negligible difference between the voltage before and after the silica sample was exposed to the laser.

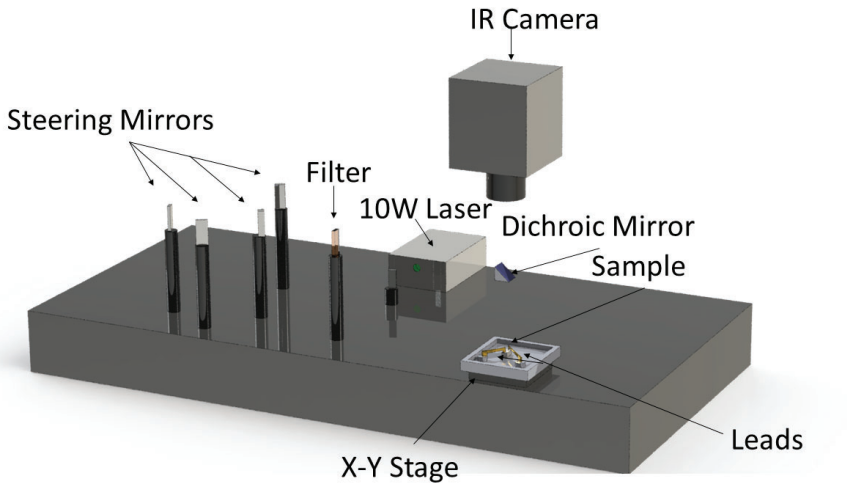

Figure 7: Custom Thermoelectric Test Setup

The CSV files with the temperature data recorded from the IR Camera was used in tandem with IR images and ImageJ software to find the temperature difference between the two leads. The camera was not calibrated for a given emissivity, because the absolute temperature did not matter, all that was needed was the temperature difference. The ΔT acquired was used with the measured steady state voltage to calculate values for the Seebeck effect. A sample IR image used during the analysis is shown in Fig. 8.

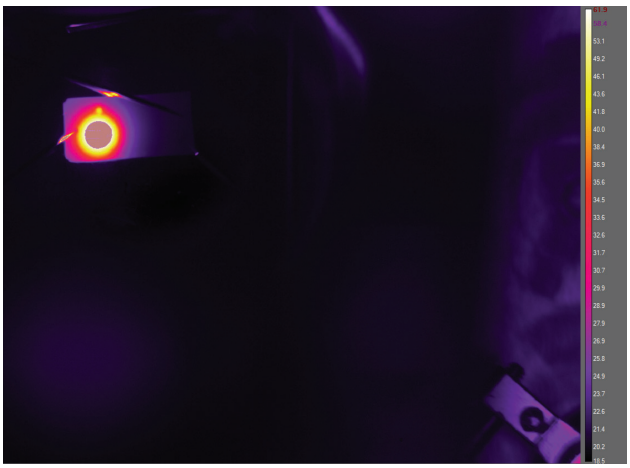

Figure 8: IR Image from the Laser Thermoelectric Characterization

III. Data Analysis

A. Fabrication

1) SLA Printing: In the SLA printing performed on the Form2 printers, two factors limited the loading of ceramic resin. The first was a density disparity between the resin and the ceramic powder. This was especially obvious in the initial resin formulation. In order to develop an effective ceramic resin, the densities of the resin and the ceramic ought to be similar. If they are not prints must be executed quickly and the resin should be mixed thoroughly using a warm resin (30°C-40°C). In tests the TMat would settle out of solution with the resin soon after a print was completed (about 3-4 hours after). The other factor that limited the TMat production was the transmissivity of the sample. Due to the darkness of BiTeSe, the laser had difficulty curing the material. This was evident in the way that 15wt% samples were flexible when they were removed from the build plate. They were not fully solid until they were exposed to an external UV light source in order to finish their curing. These two constraints limited the loading to 15wt%. While this may seem insignificant, He et al. was only able to obtain 1wt% doping [18]. Higher doping levels could be achieved with greater printer control. Greater wiper frequency– to mix resin and clear window– could solve the density problem. Similarly, greater laser power could solve the transmissivity problem. Unfortunately, printers are still very limited in what controls they give to users. A representative sample made using the Form2 is shown in Fig. 9

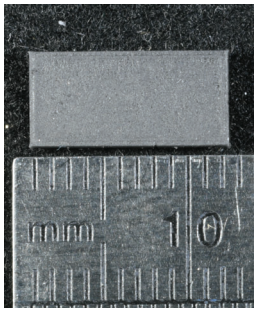

Figure 9: 5wt% Sample Made using a Formlabs Form2 Printer

2) Free Powder Sintering: Given the issues with the printer, the printer variable was removed and only used to make molds. Initially this led to the method of free powder sintering. Parts made with this method were extremely fragile, and could hardly be removed from the molds. In Fig. 10a a representative sample made in this method is shown in its mold, and similarly after removing the mold, the same sample is shown in Fig. 10b. Note how the edges have chips in them. The samples had no constitution and when leads were attached for thermoelectric characterization, any amount of torque would separate layers of the sample, removing the lead as it went. This method could be improved by sintering the samples under pressure.

(a) 100 wt% Free Powder Sintering Sample in Mold (b) 100 wt% Free Powder Sintering Sample

Figure 10: Representative Free Powder Sintering Sample

3) Bulk Curing:
a) Light Activated: Due to an inability to obtain the high doping values that were anticipated, the decision to shift to bulk curing using AM molds was made. In bulk curing the samples were initially mixed with Clear resin and then placed under a UV light. Clear 0wt% samples came out of a 30-minute cure as a solid block. At 60wt% the samples cured in thin layers (1-2 mm) after 30 minutes. The reason samples only cured into thin layers is because the UV light was only able to penetrate into the first few millimeters due to the opacity of the doped resin. Partially cured samples in the mold can be seen in Fig 11. This is included to show how unrepeatable this process was. Two molds started at the same time clearly have different extents of curing, and what is cured looks very different in composition.

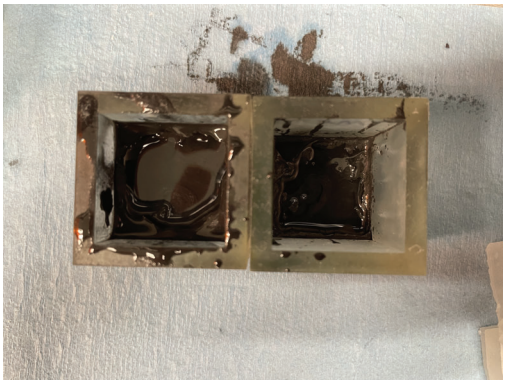

Figure 11: Partially UV Cured Doped Samples

Samples were thickened by coating the cured sections in uncured resin. This was tedious and unscientific. Using this method introduced many variables, specifically, whether or not the sample

that was being produced had a uniform dispersion of bismuth telluride. Moreover, every piece would come out slightly different. Many times, parts would cure with holes in the polymer matrix. A photo of the resulting product can be seen in Fig. 12a. Notice how the sample is disfigured, and not entirely smooth. This was the best sample that was obtained from this method. Ultimately the UV cured resin presented too many variables in the sample to continue to work with. For this reason a time activated resin replaced it in the manufacturing process.

b) Time Activated: Time cured samples were initially produced without the use of vacuum chamber for degassing. While this did produce samples, many of them contained bubbles. These bubbles became noticeable after they were cut out of the mold. This can be seen in Fig. 12b. Clearly there are several holes/ places where bubbles were trapped on the surface. Later samples were degassed by placing them in a vacuum chamber during the curing process to remove some of these bubbles. The resultant sample can be seen in Fig.12c. There are significantly less visible holes in the surface of these samples. The samples that were made with the time activated resins were able to reach a maximum of 80wt%. The resultant samples were sintered.

(a) 60 wt% Sample: Best Sample Created Using UV Activated Resin

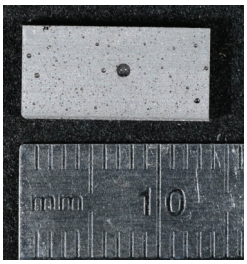

(b) Representative 80wt% Sample- No Degassing

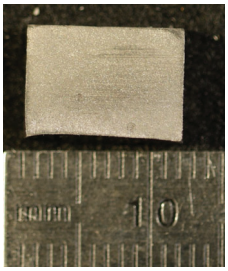

(c) Representative 80wt% Sample

Figure 12: Bulk Cured and Unsintered Samples

The sintering process involved heating the furnace to 500°C and a 5-hour hold. A lower sinter temperature of 300°C was also tested. However, the material properties of the resultant samples were inadequate. Essentially, not enough diffusion had taken place and they were not completely formed. At 500°C some samples did experience cracking, although the majority of samples were usable. Cracks were especially prevalent in thicker (greater than 20mm) parts. Similarly, many parts also experienced bloating. This is likely due to the burn off of the resin leaving voids in the sample, and the resultant void being trapped in the sample. These voids could be avoided by sintering under pressure. The density of the final parts was 3.03 g cm^{-3}. This is 39.6% of the density of the original powder which has a density of 7.642 g cm^{-3} as reported by American Elements, the supplier of the powder.

B. Microscopy

All samples were analyzed under the SEM. The samples produced with SLA are shown in Fig. 13. In Fig. 13a labeled are the reflective particles, and the pores on the surface. Similarly, in Fig. 13b there are reflective particles and more pores. These reflective particles are dispersed Bismuth Telluride powder. This was proven with an EDS scan of the material. Even without

further explanation the bright specks do represent a higher density material than the surroundings. This is true simply due to the backscatter settings used on the microscope. After thresholding the images and analyzing the resultant area percentage of particles, it was concluded that some holes can be expected. In the 5wt% samples the average area percentage was only 0.667% off from the expected value. Some of the holes likely did hold particles, while others did not, or the particles they held were smaller than the holes. This conclusion is supported with the analysis of the 15wt% samples. For the 15wt% samples, both the holes and particles were analyzed and the total added. This was done because the population of holes was so large. With this method the area percentage is greater than the expected by 37%. This confirms that holes are likely typical of any doped specimen, and that the holes are likely not the same size as the particles that were once in them. Visually this can be confirmed. In Fig. 13b, the bottom left image shows a particle that is on the verge of falling out, and the hole it occupies is much larger.

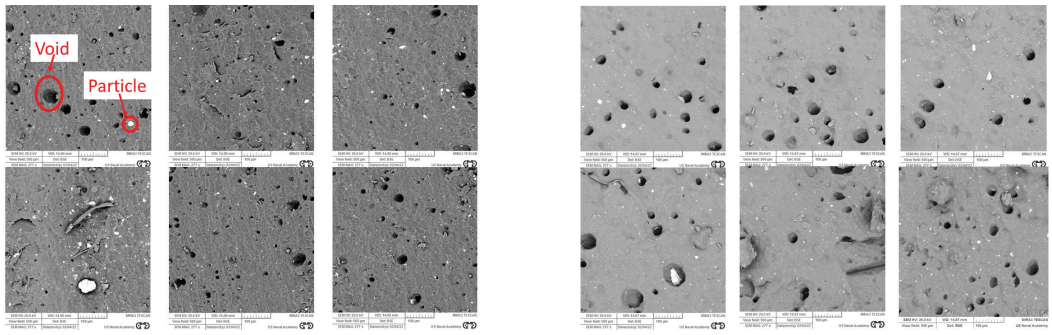

(a) Representative 5 wt% BiTeSe Doped Samples (b) Representative 15 wt% BiTeSe Doped Samples

Figure 13: Representative Doped Sample Images (View Field: 500 microns)

The holes are likely due to particles falling out of the sample. Particles could fall out from resin not fully curing and dripping off of the sample and back into the resin tray. They could fall off from handling, or even as a result of post processing. The bismuth telluride dopant is nearly 7 times as dense as the resin and it is not surprising that particle could fall out if the resin is not fully cured. All that said, 5wt% can accurately be printed. At greater percentages problems begin to develop with default printer settings. As seen with the 15wt% samples, the printer may print the sample, but it will not actually be doped to the expected level.

These inconsistencies can be attributed to the print process. With bulk curing better results were achieved. The 80wt% samples, made with bulk curing are shown in Fig. 14. These 80wt% samples do not have empty holes, but rather voids from air bubbles. In the 80wt% samples the average area of particles was greater than expected by 44.7%. The increased area was unexpected, but is likely a result of viewing more than one layer at a time. The air bubble holes present several layers to the microscopes vice one flat surface. Due to the higher weight percentage there is always a particle or two at the bottom of these holes which means that the image is not necessarily one layer, but multiple. Ultimately a larger value should be expected since the particles are three dimensional and an area analysis is a helpful check of the methods but is no means indicative of the actual composition. Since this method is biased to produce a greater percentage than reality, it is significant when that percentage is lower than expected. Therefore, a lower than expected area percentage, like that in the 15wt%, is indicative of a potentially

ineffective fabrication method.

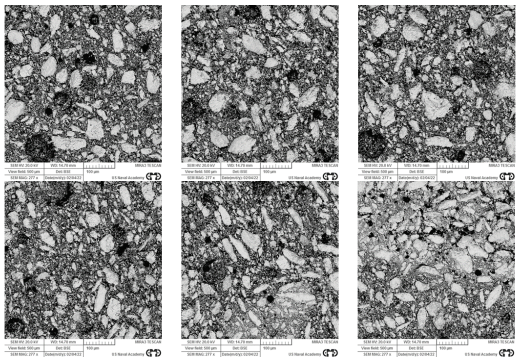

Figure 14: Representative 80 wt% BiTeSe Doped Samples (View Field: 500 microns)

The previous assumption that the bright particles are pieces BiTeSe powder was verified by EDS. The EDS map, displayed in Fig. 15, show the results of a scan on a 16wt% sample. The red and yellow highlighted sections in Fig. 15a represent the location of the corresponding energy values for bismuth and tellurium specifically. This proves that the reflective particles are in fact bismuth telluride. The graph in figure 15b shows the total number of counts represented for each energy level. The peaks are labeled according to what they represent. Gold is obviously very present, due to the sputter coating of the sample, but the bismuth and tellurium peaks are clearly distinguishable at around 3.6 keV for the tellurium and 2.4 keV for the bismuth.

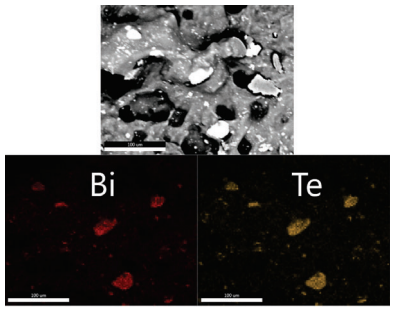

(a) Location of counts for a 15 wt% sample

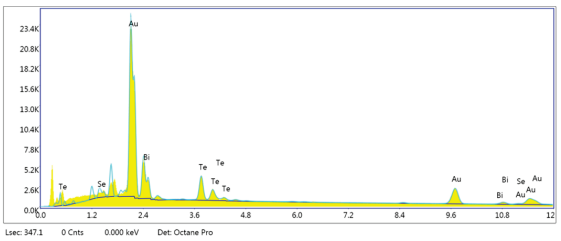

(b) Counts per energy level for a 15 wt% gold sputter coated sample

Figure 15: EDS Results for a 15wt% Sample

C. Hardness

Hardness was the only mechanical property tested. This was due to an inability to manufacture the parts needed for compression testing. Initial attempts with subtractive manufacturing failed due to an inability to machine the material with the Wire Electrical Discharge Machine or the lathe. There were also difficulties with maintaining required geometries after sintering. Similarly, time constraints did not allow for the creation of new molds that would meet ASTM specifications. Hardness tests were only run on the 80wt% samples sintered for 5 hours.

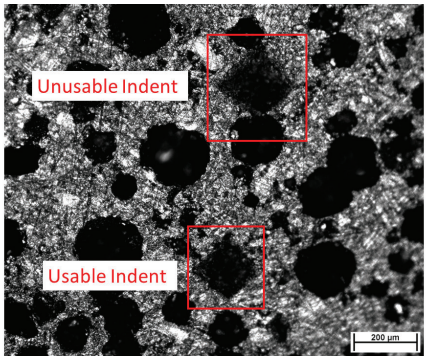

Figure 16: Typical Vickers Indents in 80wt% Sample

16 of 25 indents were considered usable. Nine indents were discarded due to their encroachment on pores and a greater than 5% difference in cross hair size. This sort of inconsistency can be seen in Fig. 19 in the Appendix. Chauvenet's Criterion was used to eliminate an additional outlier from the data set. Chauvenet's criterion was chosen as the outlier elimination method because of it's simplicity. The criterion creates a band of allowable values based off a normal distribution of the data. This data set used a 95% confidence interval. Values that fall out this 95% confidence interval are considered outliers. Ultimately, 15 data points were used. The data set with the outlier highlighted is shown in Fig. 19 in the appendix. The plotted mean line represents the mean for the data set without the outlier. The mean was 9.44 HV.5/15 and the standard deviation is 6.07. This large standard deviation makes sense, the material is non-homogeneous and it is full of pores. This fact can be seen in Fig. 16. Typical values for a conventionally manufactured material fall below 100 HV [12].

D. Thermoelectric Characterization

Samples ranging from the SLA Printed 5wt% to the Bulk Cured 80wt% were run through the PPMS TTO system. In all of them, except the bulk cured 80wt% sample that had been sintered, no measurable Seebeck effect was measured. The minimum measurable value for the PPMS system is 1 μV K^{-1}. This was likely due to the fact that the samples exhibited no electrical conductivity, and therefore had no path for the current to flow.

SLA Printed and other samples with resin were not tested with the custom laser-based system. Due to the high power of the laser, and limited control there was worry that samples would melt. Only sintered samples were tested. The acquired data can be seen in Fig. 17.

The presented data is extremely rudimentary, as many factors add to the uncertainty of these measurements. For one the multi-meter oscillated between $\pm$ 0.02 mV at all times. Similarly, the leads became more resistive as their temperature increased. Ultimately the measured values are significantly lower than those of similar materials like those manufactured by He et al. The samples produced had a max Seebeck Coefficient of 32 μV K^{-1}. He et al. had a max value of 191 μV K^{-1}, a percent difference of 83.1% [18]. The large difference could be from two factors. The first being the reliability of the results produced from the laser method used. Additionally, lower values could be a function of the large number of pores and voids in our samples. However,

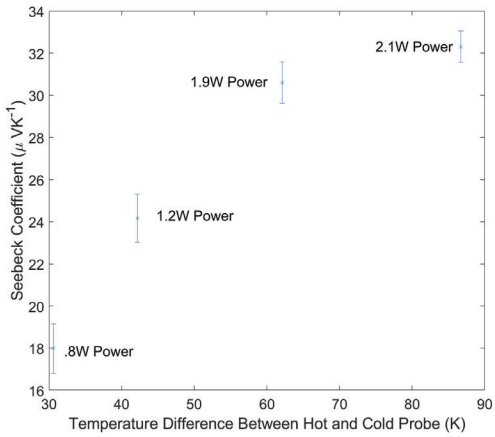

Figure 17: Seebeck Coefficient as Function of Temperature Difference between Leads

this is unlikely given that our samples are denser, 3.03 g cm^{-3} for our samples and a maximum of 2.63 g cm^{-3} for the He et al's. samples [18]. Error bars were calculated using the published uncertainty for the the camera, and the Keithly 2010 Voltmeter used with a 95% confidence interval.

The 80 wt% bulk cured and sintered sample was also tested using the Quantum Designs Thermal Transport Option. The result was a Seebeck coefficient, that is comparable to that produced by He et al. [18]. Fig. 18 shows the Seebeck coefficient as well as the thermal conductivity and resistivity and the calculated ZT. The maximum Seebeck coefficient measured was -170 μV K^{-1} at 377 K. At this Temperature He et al. reported Seebeck Coefficients in the range of 160-180 μV K^{-1}. Similarly, the figure of merit is comparable, if not greater than that reported by He et al. However, the reliability of those measurements are dependent on the thermal conductivity, which is dependent on emissivity. The error bars in Fig. 18 are large due to difficulty in measuring the radiative heat loss. More accurate measurements for thermal conductivity could be performed and a more thorough analysis of the thermal conductivity could add more confidence to the results. The ZT error bars is a combination of the known error from thermal conductivity, Seebeck coefficient, and resistivity. The error for the latter two is minimal and not included on the plots, but is a function of heater current error from the digital to analog converter,a 20% combined error in the estimation of surface area and emissivity, and a 10% error assumption heat leaked from heater shoes. All error calculations were done in accordance with instructions laid out in the physical properties measurement system- thermal transport option manual [48].

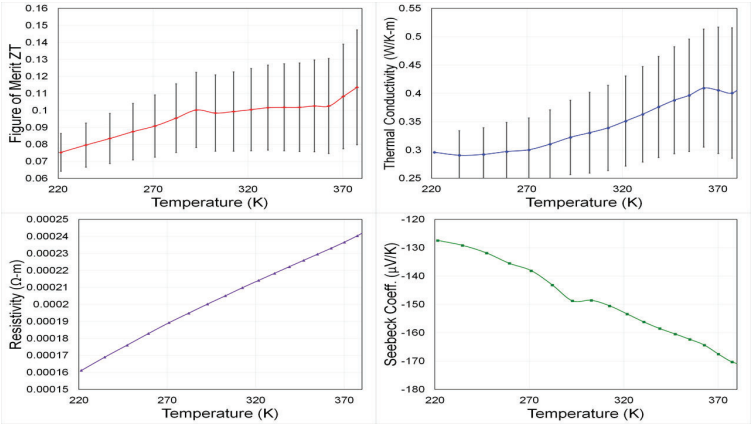

Figure 18: Figure of Merit, Thermal Conductivity, Seebeck Coefficient, and Resistivity all plotted as a function of temperature

IV. Conclusions

The main objective of this study was to develop and evaluate a manufacturing process that allowed for the creation of custom geometries and relied on additive manufacturing. The next objective was to characterize the samples created with this newly developed method. These objectives were met.

Despite mild improvements since 2015 when He et al. attempted to use SLA to print a thermoelectric, stereolithography of TMats and other ceramic materials is still constrained by printer technology. Until more control is given to users the direct production of TMats using SLA will be limited.

Increasing the weight percentage of dopants still leads to a curable product, but printers need to be developed that allow users to alter all the controls. The results demonstrated here offer promise for others looking to dope a resin with metal or ceramic particles. The image analysis shows that at 5wt%, a powder 7 times as dense as a resin can be effectively mixed and printed. At 15wt% holes will begin to form due to inadequate printer settings.

However, SLA's improved dimensional accuracy still has potential to produce parts using molds. Whether that is through bulk curing or through the use of sintering and ceramic molds. Bulk cured parts are comparable TMats to those made by He et al, and they require no special printer to make. The resultant material is not terribly hard though with a hardness of about 9HV.5/15.

Ultimately, additive manufacturing does offer a solution to some of the manufacturing problems, but does so at a cost. Resultant parts are extremely porous, lacking both mechanical and significant thermoelectric properties. Future investigation into the mechanical properties is encouraged, especially, work to solve the problem of voids created during the sintering process should be pursued.

APPENDIX
CHAUVENET CRITERION

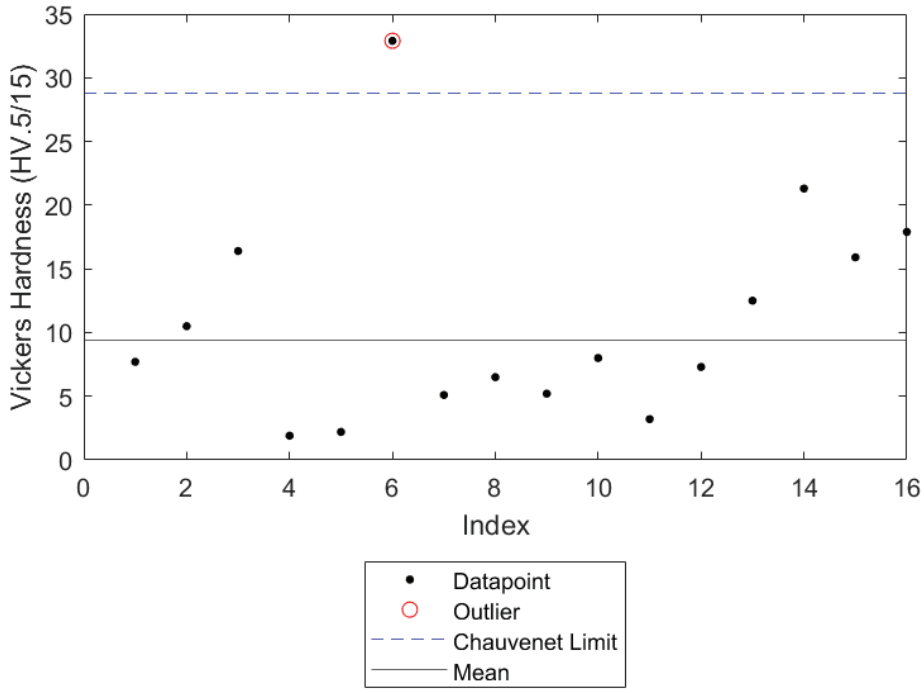

Figure 19: Vickers Hardness Data for 80wt% Sample Sintered for 5 hours

REFERENCES

[1] T. J. Seebeck, "Ueber die magnetische Polarisation der Metalle und Erze durch Temperaturdifferenz," *Annalen der Physik*, vol. 82, no. 3, pp. 253–286, 1826. [Online]. Available: http://doi.wiley.com/10.1002/andp.18260820302

[2] M. A. Zoui, S. Bentouba, J. G. Stocholm, and M. Bourouis, "A Review on Thermoelectric Generators: Progress and Applications," *Energies*, vol. 13, no. 14, p. 3606, Jul. 2020. [Online]. Available: https://www.mdpi.com/1996-1073/13/14/3606

[3] J. Cedar, A. Drummond, C. Burns, and M. Nowicki, "Portable combustion device utilizing thermoelectrical generation," Patent US20 130 112 187A1, May, 2013. [Online]. Available: https://patents.google.com/patent/US20130112187A1/en

[4] "Dyson energy bracelet a good call," Jun. 2009. [Online]. Available: https://newatlas.com/dyson-energy-bracelet/12040/

[5] "Radioisotope thermoelectric generators of the U. S. Navy. Volume 10. Final report 1 January 1976–1 July 1978," Naval Nuclear Power Unit, Fort Belvoir, VA (USA), United States, Technical Report AD-A-057483, Jul. 1978.

[6] D. M. Rowe, *Thermoelectrics handbook: macro to nano*. CRC/Taylor & Francis, OCLC: 813844577. [Online]. Available: http://www.crcnetbase.com/isbn/9781420038903

[7] M. Hong, T. C. Chasapis, Z.-G. Chen, L. Yang, M. G. Kanatzidis, G. J. Snyder, and J. Zou, "n -type bi 2te3-x sex nanoplates with enhanced thermoelectric efficiency driven by wide-frequency phonon scatterings and synergistic carrier scatterings," vol. 10, no. 4, pp. 4719–4727. [Online]. Available: https://pubs.acs.org/doi/10.1021/acsnano.6b01156

[8] B. Poudel, Q. Hao, Y. Ma, Y. Lan, A. Minnich, B. Yu, X. Yan, D. Wang, A. Muto, D. Vashaee, X. Chen, J. Liu, M. S. Dresselhaus, G. Chen, and Z. Ren, "High-thermoelectric performance of nanostructured bismuth antimony telluride bulk alloys," vol. 320, no. 5876, pp. 634–638. [Online]. Available: https://www.sciencemag.org/lookup/doi/10.1126/science.1156446

[9] "Fundamentals of engineering thermodynamics."

[10] A. F. Ioffe, *Semiconductor thermoelements, and, Thermoelectric cooling*. Infosearch.

[11] N. Jaziri, A. Boughamoura, J. Müller, B. Mezghani, F. Tounsi, and M. Ismail, "A comprehensive review of thermoelectric generators: Technologies and common applications," p. S2352484719306997. [Online]. Available: https://linkinghub.elsevier.com/retrieve/pii/S2352484719306997

[12] A. A. Wereszczak and E. D. Case, "Mechanical response of thermoelectric materials," pp. ORNL/TM–2015/227, 1 187 907. [Online]. Available: http://www.osti.gov/servlets/purl/1187907/

[13] C. J. Smithells, W. F. Gale, and T. C. Totemeier, *Smithells metals reference book*, 8th ed. Elsevier Butterworth-Heinemann.

[14] E. Ryshkewitch, "Compression strength of porous sintered alumina and zirconia.: 9th communication to ceramography," vol. 36, no. 2, pp. 65–68. [Online]. Available: http://doi.wiley.com/10.1111/j.1151-2916.1953.tb12837.x

[15] C. Reynaud and F. Thevenot, "Porosity dependence of mechanical properties of porous sintered SiC. verification of the minimum solid area model," vol. 19, no. 10, pp. 871–874. [Online]. Available: http://link.springer.com/10.1023/A:1006741616088

[16] J. Hostaša, W. Pabst, and J. Matějíček, "Thermal conductivity of al2o3-ZrO2 composite ceramics," vol. 94, no. 12, pp. 4404–4409. [Online]. Available: http://doi.wiley.com/10.1111/j.1551-2916.2011.04875.x

[17] C. Oztan, S. Ballikaya, U. Ozgun, R. Karkkainen, and E. Celik, "Additive manufacturing of thermoelectric materials via fused filament fabrication," vol. 15, pp. 77–82. [Online]. Available: https://linkinghub.elsevier.com/retrieve/pii/S2352940719300034

[18] M. He, Y. Zhao, B. Wang, Q. Xi, J. Zhou, and Z. Liang, "3D Printing Fabrication of Amorphous Thermoelectric Materials with Ultralow Thermal Conductivity," *Small*, vol. 11, no. 44, pp. 5889–5894, Nov. 2015. [Online]. Available: http://doi.wiley.com/10.1002/smll.201502153

[19] M. Telkes, "Method of assembling thermoelectric generators," patentus 2 289 152A.

[20] Crystal technology feature and advantages.

[21] N. Maegawa, H. Okada, M. Tsuzaki, Y. Sakai, K. Shimoda, T. Komatsu, S. Murase, H. Inoue, and M. Sagawa, "Method of fabricating a thermoelectric module," patentus 5 950 067A.

[22] Y. Thimont and S. LeBlanc, "The impact of thermoelectric leg geometries on thermal resistance and power output," vol. 126, no. 9, p. 095101. [Online]. Available: http://aip.scitation.org/doi/10.1063/1.5115044

[23] G. Shu, X. Ma, H. Tian, H. Yang, T. Chen, and X. Li, "Configuration optimization of the segmented modules in an exhaust-based thermoelectric generator for engine waste heat recovery," vol. 160, pp. 612–624. [Online]. Available: https://linkinghub.elsevier.com/retrieve/pii/S0360544218312404

[24] H. Tian, N. Jiang, Q. Jia, X. Sun, G. Shu, and X. Liang, "Comparison of segmented and traditional thermoelectric generator for waste heat recovery of diesel engine," vol. 75, pp. 590–596. [Online]. Available: https://linkinghub.elsevier.com/retrieve/pii/S1876610215012291

[25] C. L. Cramer, W. Li, Z.-H. Jin, J. Wang, K. Ma, and T. B. Holland, "Techniques for mitigating thermal fatigue degradation, controlling efficiency, and extending lifetime in a ZnO thermoelectric using grain size gradient FGMs," vol. 47, no. 1, pp. 866–872. [Online]. Available: http://link.springer.com/10.1007/s11664-017-5879-9

[26] F42 Committee, "Terminology for additive manufacturing - general principles - terminology." [Online]. Available: http://www.astm.org/cgi-bin/resolver.cgi?ISOASTM52900-15

[27] D. Puppi, A. M. Piras, A. Pirosa, S. Sandreschi, and F. Chiellini, "Levofloxacin-loaded star poly(-caprolactone) scaffolds by additive manufacturing," vol. 27, no. 3, p. 44. [Online]. Available: http://link.springer.com/10.1007/s10856-015-5658-1

[28] S. H. Huang, P. Liu, A. Mokasdar, and L. Hou, "Additive manufacturing and its societal impact: a literature review," vol. 67, no. 5, pp. 1191–1203. [Online]. Available: http://link.springer.com/10.1007/s00170-012-4558-5

[29] K. Schlichting, T. Novak, and A. Heinrich, "Additive manufacturing of tunable lenses," C. E. Tabor, F. Kajzar, T. Kaino, and Y. Koike, Eds., p. 1010116.

[30] S. Verploegh, M. Coffey, E. Grossman, and Z. Popovic, "Properties of 50–110-GHz waveguide components fabricated by metal additive manufacturing," vol. 65, no. 12, pp. 5144–5153. [Online]. Available: http://ieeexplore.ieee.org/document/8120160/

[31] N. Sridharan, Y. Chen, P. Nandwana, R. M. Ulfig, D. J. Larson, and S. S. Babu, "On the potential mechanisms of to + decomposition in two phase titanium alloys during additive manufacturing: a combined transmission kikuchi diffraction and 3d atom probe study," vol. 55, no. 4, pp. 1715–1726. [Online]. Available: http://link.springer.com/10.1007/s10853-019-03984-w

[32] B. E. Carroll, T. A. Palmer, and A. M. Beese, "Anisotropic tensile behavior of ti–6al–4v components fabricated with directed energy deposition additive manufacturing," vol. 87, pp. 309–320. [Online]. Available: https://linkinghub.elsevier.com/retrieve/pii/S135964541400980X

[33] A. El-Desouky, M. Carter, M. Mahmoudi, A. Elwany, and S. LeBlanc, "Influences of energy density on microstructure and consolidation of selective laser melted bismuth telluride thermoelectric powder," *Journal of Manufacturing Processes*, vol. 25, pp. 411–417, Jan. 2017. [Online]. Available: https://linkinghub.elsevier.com/retrieve/pii/S1526612516301797

[34] Y. Thimont, L. Presmanes, V. Baylac, P. Tailhades, D. Berthebaud, and F. Gascoin, "Thermoelectric higher manganese silicide: Synthetized, sintered and shaped simultaneously by selective laser sintering/melting additive manufacturing technique," vol. 214, pp. 236–239. [Online]. Available: https://linkinghub.elsevier.com/retrieve/pii/S0167577X17317858

[35] Y. Yan, H. Ke, J. Yang, C. Uher, and X. Tang, "Fabrication and thermoelectric properties of n-type $CoSb_{2.85}te_{0.15}$ using selective laser melting," vol. 10, no. 16, pp. 13 669–13 674. [Online]. Available: https://pubs.acs.org/doi/10.1021/acsami.8b01564

[36] X. Chen, Z. Zhou, Y.-H. Lin, and C. Nan, "Thermoelectric thin films: Promising strategies and related mechanism on boosting energy conversion performance," vol. 6, no. 3, pp. 494–512. [Online]. Available: https://linkinghub.elsevier.com/retrieve/pii/S2352847820300095

[37] D. Madan, Z. Wang, A. Chen, R.-c. Juang, J. Keist, P. K. Wright, and J. W. Evans, "Enhanced Performance of Dispenser Printed MA n-type Bi_2Te_3 Composite Thermoelectric Generators," *ACS Applied Materials & Interfaces*, vol. 4, no. 11, pp. 6117–6124, Nov. 2012. [Online]. Available: https://pubs.acs.org/doi/10.1021/am301759a

[38] N. Su, P. Zhu, Y. Pan, F. Li, and B. Li, "3d-printing of shape-controllable thermoelectric devices with enhanced output performance," vol. 195, p. 116892. [Online]. Available: https://linkinghub.elsevier.com/retrieve/pii/S0360544219325873

[39] S. Kee, M. A. Haque, D. Corzo, H. N. Alshareef, and D. Baran, "Self-Healing and Stretchable 3D-Printed Organic Thermoelectrics," *Advanced Functional Materials*, vol. 29, no. 51, p. 1905426, Dec. 2019. [Online]. Available: https://onlinelibrary.wiley.com/doi/abs/10.1002/adfm.201905426

[40] J. Wang, H. Li, R. Liu, L. Li, Y.-H. Lin, and C.-W. Nan, "Thermoelectric and mechanical properties of PLA/bi0·5sb1·5te3 composite wires used for 3d printing," vol. 157, pp. 1–9. [Online]. Available: https://linkinghub.elsevier.com/retrieve/pii/S0266353817327823

[41] Yah Aw, Cheow Yeoh, Muhammad Idris, Pei Teh, Khairul Hamzah, and Shulizawati Sazali, "Effect of printing parameters on tensile, dynamic mechanical, and thermoelectric properties of FDM 3d printed CABS/ZnO composites," vol. 11, no. 4, p. 466. [Online]. Available: http://www.mdpi.com/1996-1944/11/4/466

[42] C. Hull, "Apparatus for production of three-dimensional objects by stereolithography," patentus 4 575 330A.

[43] J. Sootsman, D. Chung, and M. Kanatzidis, "New and old concepts in thermoelectric materials," vol. 48, no. 46, pp. 8616–8639. [Online]. Available: http://doi.wiley.com/10.1002/anie.200900598

[44] X. Shi, J. Yang, J. R. Salvador, M. Chi, J. Y. Cho, H. Wang, S. Bai, J. Yang, W. Zhang, and L. Chen, "Multiple-filled skutterudites: High thermoelectric figure of merit through separately optimizing electrical and thermal transports," vol. 133, no. 20, pp. 7837–7846. [Online]. Available: https://pubs.acs.org/doi/10.1021/ja111199y

[45] A. U. Khan, K. Kobayashi, D.-M. Tang, Y. Yamauchi, K. Hasegawa, M. Mitome, Y. Xue, B. Jiang, K. Tsuchiya, D. Golberg, Y. Bando, and T. Mori, "Nano-micro-porous skutterudites with 100% enhancement in ZT for high performance thermoelectricity," vol. 31, pp. 152–159. [Online]. Available: https://linkinghub.elsevier.com/retrieve/pii/S2211285516304979

[46] K. B. Masood, P. Kumar, R. A. Singh, and J. Singh, "Odyssey of thermoelectric materials: foundation of the complex structure," vol. 2, no. 6, p. 062001. [Online]. Available: https://iopscience.iop.org/article/10.1088/2399-6528/aab64f

[47] W. Xie, S. Wang, S. Zhu, J. He, X. Tang, Q. Zhang, and T. M. Tritt, "High performance bi2te3 nanocomposites prepared by single-element-melt-spinning spark-plasma sintering," vol. 48, no. 7, pp. 2745–2760. [Online]. Available: http://link.springer.com/10.1007/s10853-012-6895-z

[48] *Physical Property Measurement System AC Transport Option User's Manual*, 5th ed.